Experiments on a wireless power transfer system for wearable device with sol-gel thin-film PZT

Experiments on a wireless power transfer system for wearable device with sol-gel thin-film PZT

Binh Duc Truong[1], Dixiong Wang[2], Tiancheng Xue[1], Susan Trolier-McKinstry[2] and Shad Roundy[1]

[1] University of Utah, Department of Mechanical Engineering, 1495 E 100 S, Salt Lake City, UT, United States of America, and
[2] Pennsylvania State University, Materials Science and Engineering Department and Materials Research Institute, Millennium Science Complex, University Park, PA, United States of America.

E-mail: shad.roundy@utah.edu

Abstract. This paper presents experiments on a low-frequency wireless power transfer system (WPTS) using a piezoelectric transducer with a magnet tip mass as a receiver. The thin-film piezoelectric bimorph cantilever is fabricated by sol-gel processing with the aim to miniaturize the system for wearable applications. The device couples an applied electromagnetic field to the mechanical transverse vibration of the beam, which then induces a voltage across a load resistance connected to the electrical ports. This coupled mechanism is therefore referred to as the magneto-mechano-electric (MME) effect. A power of 3.4 μW is generated in a resistance of 200 kΩ at a magnetic flux density of 100.3 μT. The potential of utilizing the same piezoelectric resonator for both energy harvesting and wireless power transmission modes is shown.

1. Introduction

Energy harvesting (EH) and WPTS are promising alternatives to batteries for powering consumer electronics [1, 2]. Advanced EH techniques have been developed to scavenge energy from body motion or heat using electromechanical/electrodynamic resonators or thermoelectric generators [3, 4] for utilization in smart, secure systems for human health monitoring. While the frequency of human motion is relatively low (a few Hz), the resonance frequency of vibrational harvesters is much higher (usually around hundreds Hz), degrading the effectiveness of these harvesters in practice. However, frequency up-converting piezoelectric energy harvesters with magnetic plucking configurations can overcome this obstacle [5, 6]. In previous work, a harvester architecture consisting of 10 PZT thin-film beams generated approximately 40 μW under a sinusoidal excitation of 25° and 0.8 second [7].

WPTSs are also widely used to power implantable bio-electronics [8]. Resonantly coupled inductive coils typically operate at a frequency range of MHz [9–11]. By contrast, a near-field WPTS utilizing a permanent magnet and a piezoelectric structure as a receiver can reduce the resonance frequency to below 1 kHz [12]. This lower frequency allows the safe application of much higher external magnetic flux densities to humans [13, 14]. The potential application of piezoelectric resonators for harvesting power from ambient low-frequency magnetic fields has been reported by several groups, using off-the-shelf devices [15].

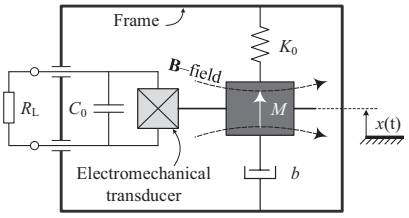

Figure 1: A generic model of an electromechanical-based WPTS.

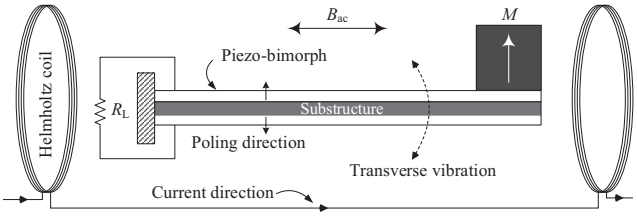

Figure 2: Schematic of Helmholtz coil transmitter and piezoelectric/magnet receiver.

This study investigates the performance of a WPTS based on a PZT thin-film beam fabricated by sol-gel processing, with the aim to miniaturize the system and unify both EH and WPTS into a single wearable device. The central concepts of the unified approach, the process for fabricating PZT thin-film structures and the fundamental operation of the low-frequency WPTS, are discussed.

2. Device concept and system description

The device concept and generic model of an electromechanical-based WPTS is shown in Figure 1. The mechanical part of the transducer can be linearized and characterized by a mass-spring-damper system where the inertial mass, the parasitic damping coefficient and the stiffness are denoted as M, b and K_0 respectively. The coupling between the mechanical and electrical domain is modeled as a linear two-port transducer [16–19]. The mass M is also a permanent magnet (its magnetization direction is marked by a white arrow in the Figure). When an external magnetic flux density is applied, the interactions between the magnet mass and the $\mathbf{B}-$field or the magnetic flux gradient cause a moment and/or a force acting on the resonator and result in the relative displacement $x(t)$ between the mass and the frame. If an electrostatic or a piezoelectric generator is utilized, C_0 is the transducer nominal capacitance. The electrical terminals are typically connected to a load resistance R_{L} in order to investigate the device performance. In the case in which an electromagnetic resonator is used, the electrical domain is modeled as an inductance L_0 in series with the load R_{L} (not shown in the Figure). Furthermore, if there is no power transmitted, the receiver can also harvest the kinetic energy when the frame is accelerated or the magnet mass is magnetically plucked.

In this paper, a circular Helmholtz coil was used as a transmitter and a bimorph piezoelectric cantilever beam with a magnet tip mass as a receiver. A simplified schematic of this structure is shown in Figure 2 where the two piezoelectric layers are configured in a series connection. A uniform magnetic field generated along the longitudinal axis of the beam (i.e., perpendicular to the magnetization direction) induces a pure torque on the magnet mass. As a consequence, the piezoelectric cantilever vibrates in the transverse direction and produces an output voltage across the resistor.

3. Fabrication method and measurement results

The cross sectional schematic and a SEM picture of the PZT beam used in experiments are depicted in Figure 3, where two 3 μm 2 % Mn-doped $Pb(Zr_{0.52}Ti_{0.48})O_3$ thin films were spin coated on a 50 μm Nickel foil passivated with 30 nm HfO_2 (as a barrier layer against Ni oxidation) and 100 nm $LaNiO_3$ (as a seed layer for {001} oriented PZT and the bottom electrode). The detailed fabrication parameters of PZT films and the substrates were described by Yeo *et. al.* [20]. The total thickness of the beam is 56 μm with 2×3 μm PZT, approximately. The PZT films have a dielectric constant of 480 and a tangent loss of 0.032. The piezoelectric constant ($e_{31,\mathrm{f}}$)

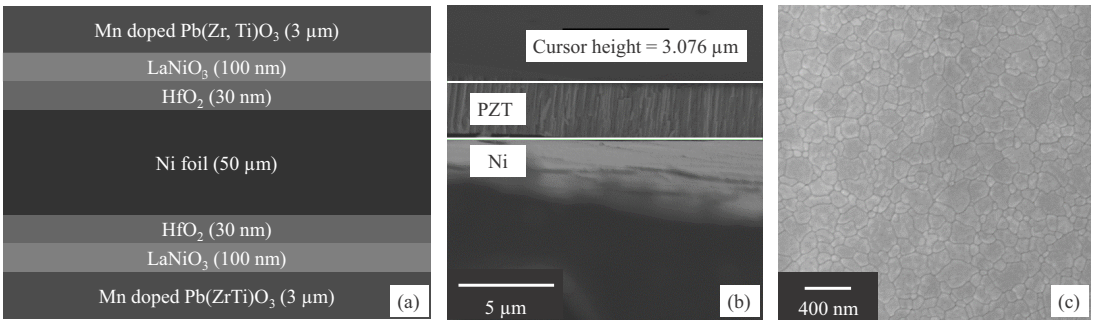

Figure 3: (a) Schematic and (b) Scanning electron microscope (SEM) picture of the PZT beam cross section. (c) Close-up view of a top surface.

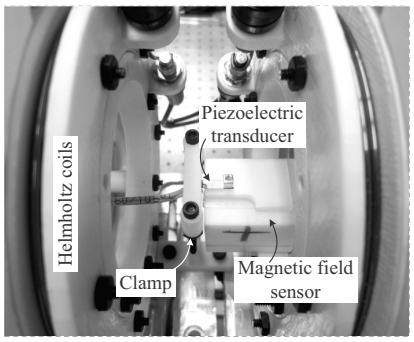

Figure 4: Helmholtz coil (transmitter) and piezoelectric/magnet generator (receiver) used in the experiments.

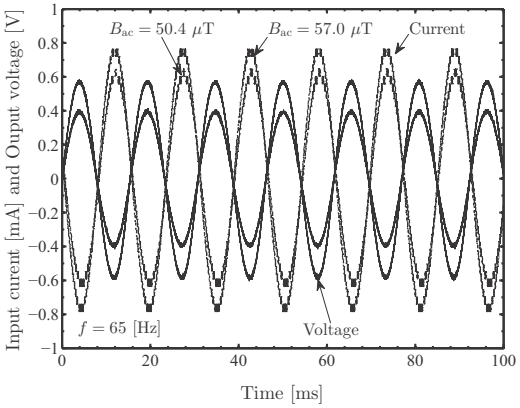

Figure 5: Waveforms of the current input to the Helmholtz coil and the output voltage $V_{\rm L}$ induced in a load resistance of $R_{\rm L} = 200$ kΩ in two cases $B_{\rm ac} = 50.4\ \mu$T and $57.0\ \mu$T.

of the films are -8.2 C/m^2 measured by a flexure wafer method [21]. The nominal capacitance of the piezoelectric generator is $C_0 \approx 3.7$ nF.

Figure 4 shows the experimental prototype of the Helmholtz transmitting coil and the piezoelectric/magnet receiver. The beam is clamped at one end by a plastic anchor while the magnet mass is fixed on the tip using a nonconductive glue. The Helmholtz coil is driven by a Rigol power amplifier. A Tektronix function generator acts as a control unit for adjusting the driving frequency and the input power. The output voltage across the load $R_{\rm L}$ is accumulated by a data acquisition (DAQ) unit that communicates to a computer via the USB protocol. The average power is then computed as $P_{\rm L} = \langle V_{\rm L}^2 \rangle / R_{\rm L}$ where $\langle V_{\rm L}^2 \rangle$ is the mean of the values $(V_{\rm L}(t))^2$. The $\mathbf{B}-$field strength is measured by an AC milligauss meter.

Figure 5 presents the sinusoidal waveforms of the current input to the coil and the voltage induced in the load with the driving frequency of $f = 65$ Hz. As expected, higher input current to the Helmoltz coil leads to higher output voltage across the load resistor. Since the frequency used here is close to the mechanical resonance, the input current and the output voltage are nearly in the opposite phase (i.e., the phase difference between them is $\Delta\phi = \pi$). This indicates that $|\cos\Delta\phi| = 1$ and the power delivered to the load is maximized. We also observe that $\Delta\phi$

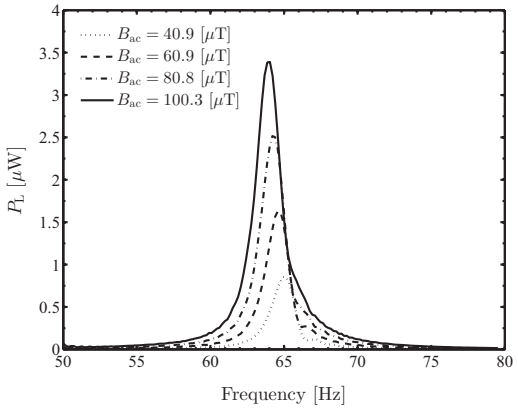

Figure 6: Frequency responses of the transferred power with different external **B**−field amplitudes and $R_L = 200$ kΩ.

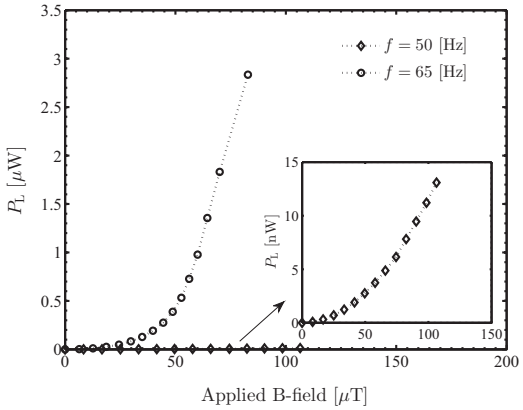

Figure 7: **B**−field responses of the transferred power with fixed driving frequencies and $R_L = 200$ kΩ.

changes and the output voltage drops significantly as the driving frequency f is adjusted. For instance, with the same input current amplitude of 0.6 mA, the peak generated voltage is about 0.3 V at $f = 67$ Hz, which is 25% lower than that obtained by $f = 65$ Hz, approximately.

Figure 6 shows the frequency responses of the system with different **B**−field amplitudes ranging from about 40 μT to 100 μT. A slightly softening effect is observed since the resonance frequency reduces as the applied field increases. This can be explained by the slight curvature in the beam caused by the fabrication/assembly processes and the imperfect rigidity of the clamp. The maximum power of 3.4 μW is achieved at B_{ac}=100.3 μT and $f = 64$ Hz.

Figure 7 presents the behavior of the output power P_L in terms of the external **B**−field at two different driving frequencies $f = 50$ Hz and $f = 65$ Hz. It is obvious that operating off-resonance (i.e., $f = 50$ Hz) leads to a dramatic reduction of the transferred power to a few nW. In contrast, at resonance, a power of 2.8 μW is obtained at B_{ac}=82 μT. In principle, P_L can be approximated as a quadratic function of B_{ac} when the displacement of the beam is small. However, as the **B**−field strength increases, nonlinearities result in resonance frequency shifts and the quadratic nature of the curve changes. All these nonlinear behaviors need to be taken into consideration for complete device design and further optimization. In particular, the system must track the mechanical resonance frequency in order to maintain a sufficient power delivered to a load.

4. Conclusions

The feasibility of a low-frequency WPTS was demonstrated using a PZT thin-film with a magnet tip mass as a receiver. Further improvements to the system such as increasing the size of the magnet tip mass to increase the coupling between the electromagnetic and mechanical domains, or optimizing the fabricated beam dimensions (i.e. increasing the thickness of the deposited PZT) are possible. Further applications of this research include operating a piezoelectric-based wearable device in dual modes of vibrational EH and wireless power transfer.

Acknowledgment

The authors would like to thank Erik Andersen for his valuable comments and suggestions. This work was supported by the National Science Foundation ASSIST Nanosystems ERC under Award Number EEC-1160483.

References

[1] Beeby S P, Tudor M J and White N M 2006 *Measurement Science and Technology* **17** R175–R195
[2] Karalis A, Joannopoulos J and Soljačić M 2008 *Annals of Physics* **323** 34 – 48 ISSN 0003-4916 Special Issue
[3] von Buren T, Mitcheson P D, Green T C, Yeatman E M, Holmes A S and Tröster G 2006 *IEEE Sensors Journal* **6** 28–38 ISSN 1530-437X
[4] Mitcheson P 2010 *IEEE EMBC* pp 3432–3436
[5] Xue T and Roundy S 2015 *Journal of Physics: Conference Series* **660** 012098
[6] Xue T and Roundy S 2017 *Sensors and Actuators A: Physical* **253** 101 – 111 ISSN 0924-4247
[7] Xue T, Yeo H G, Trolier-McKinstry S and Roundy S 2018 *Smart Materials and Structures* **27** 085026
[8] Agarwal K, Jegadeesan R, Guo Y X and Thakor N V 2017 *IEEE Reviews in Biomedical Engineering* **10** 136–161 ISSN 1937-3333
[9] Kurs A, Karalis A, Moffatt R, Joannopoulos J D, Fisher P and Soljačić M 2007 *Science* **317** 83–86 ISSN 0036-8075
[10] Sample A P, Meyer D T and Smith J R 2011 *IEEE Transactions on Industrial Electronics* **58** 544–554 ISSN 0278-0046
[11] Pacini A, Costanzo A, Aldhaher S and Mitcheson P D 2017 *IEEE Transactions on Microwave Theory and Techniques* **65** 5367–5376 ISSN 0018-9480
[12] Challa V R, Mur-Miranda J O and Arnold D P 2012 *Smart Materials and Structures* **21** 115017
[13] IEEE 2002 *IEEE Std C95.6-2002* 1–0
[14] IEEE 2006 *IEEE Std C95.1-2005 (Revision of IEEE Std C95.1-1991)* 1–238
[15] Paprotny I, Xu Q, Chan W W, White R M and Wright P K 2013 *IEEE Sensors Journal* **13** 190–201 ISSN 1530-437X
[16] Tilmans H A C 1996 *Journal of Micromechanics and Microengineering* **6** 157–176
[17] Roundy S and Wright P K 2004 *Smart Materials and Structures* **13** 1131–1142
[18] Erturk A and Inman D J 2009 *Smart Materials and Structures* **18** 025009
[19] Halvorsen E 2016 *ArXiv e-prints* (*Preprint* 1603.01909)
[20] Yeo H G and Trolier-McKinstry S 2014 *Journal of Applied Physics* **116** 014105
[21] Shepard J, Moses P and Trolier-McKinstry S 1998 *Sensors and Actuators A: Physical* **71** 133 – 138 ISSN 0924-4247